Observation of Large-Angle Quasimonoenergetic Electrons from a Laser Wakefield

D. Kaganovich,* D. F. Gordon, and A. Ting
Plasma Physics Division, Naval Research Laboratory, Washington, D.C. 20375, USA
(Received 15 January 2008; published 29 May 2008)

A relativistically intense laser pulse is focused into a helium jet and quasimonoenergetic electrons emitted at a 40° angle with respect to the laser axis are observed. The average electron energy is between 1 and 2 MeV and the total accelerated charge is about 1 nC emitted in a 10° cone angle. Three dimensional particle-in-cell simulations reproduce key features of the experimental results and show that the interaction between ionization heating and nonlinear cavitation wakefields is responsible for the acceleration.

DOI: 10.1103/PhysRevLett.100.215002 PACS numbers: 52.38.Kd, 41.75.Jv

The laser wakefield accelerator (LWFA) [1–3] is one of several advanced accelerator concepts that takes advantage of the extremely high electric fields that can be supported in a plasma. The LWFA produces a large amplitude plasma wave whose phase velocity approaches the speed of light and can trap electrons and accelerate them to high energies. Quasimonoenergetic acceleration of electrons from the background plasma has been observed recently in simulations [4–6] and experiments [7–9] operating in the so-called ''bubble'' regime of LWFA. The stability of the accelerator can be improved by controlling the initial injection [10], and the energy can be increased by guiding the laser pulse in a plasma channel [11]. The energy can be increased even further by staging multiple plasma channel accelerator sections [12]. It is evident that injection and staging are key issues for a stable and practical laser wakefield accelerator.

Recent theoretical and simulation work [13,14] shows that with proper choice of laser, plasma, and injection parameters, it may be possible to produce accelerated electron bunches with modest energy spread and short bunch length even though the initial bunch length or energy spread is large. This makes it possible to consider a much wider list of injection schemes. Schemes that allow for a noncollinear geometry with respect to the injection and acceleration lasers are desirable for practical reasons, such as the possibility of using two noncollinear laser beams for injection and acceleration for easier alignment of the injection electron beam into the acceleration structure. Although such geometry is achieved via the Laser Ionization and Ponderomotive Acceleration (LIPA) [15] and High Density LIPA (HD-LIPA) [16] schemes, these require very high laser power and yield low charge. We have recently observed in our experiments unexpected off-axis, well directed, quasimonoenergetic, high charge electrons generated in a laser wakefield acceleration environment, using relatively modest laser power and intensities in a helium jet plasma. These electrons could be a very desirable source of injection electrons for the first stage of a practical high-energy laser driven accelerator.

The experimental setup is similar to our previous experiments [12,16] with the following modifications as shown in Fig. 1. This system measures both the angular distribution of the ejected electrons and the electron energy spectrum for any angle between 0° and 50°. The main part of the system is the electron spectrometer that is mounted on a rotational stage in the vacuum chamber. The axis of rotation is designed to coincide with the position of the gas jet, where the electrons are generated. A collimator and an electromagnet are mounted on the rotational stage and a scintillator plate is banded around the backside of the electromagnet. Clockwise rotation of the stage from 0° to 50° allows scanning of the electron energy distribution for this range of angles, whereas counterclockwise rotation opens the entire scintillator area for angular distribution studies.

In the experimental studies we have used both helium and nitrogen gases and have been able to change the

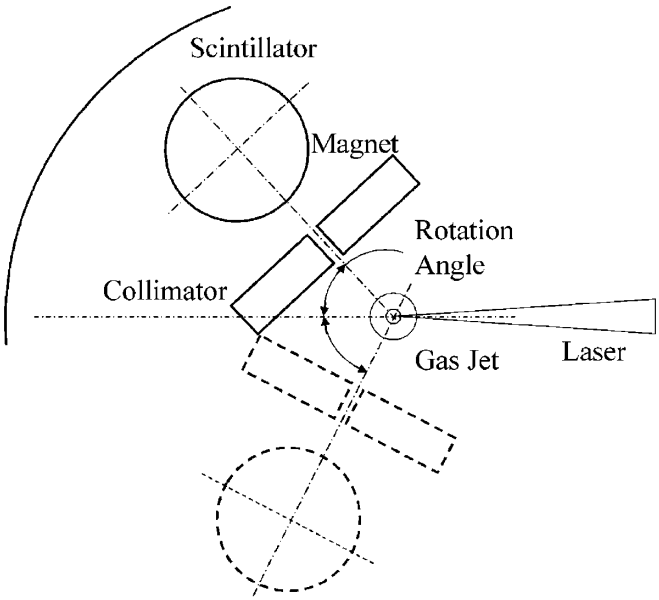

FIG. 1. Experimental system with rotational arm electron spectrometer.

plasma densities from 10^{18} cm^{-3} to 5×10^{19} cm^{-3}. The plasma density was measured by interferometry and Raman backscattering.

The 50 fs laser beam was focused to the 0.5 mm diameter gas jet using an $f/10$ off-axis parabolic mirror. The jet has 100 μm density gradient ramps and 300 μm plateau in the center. The power of the laser was continuously changed from 2 to 10 TW, corresponding to a peak laser intensity that ranged from 1 to 5×10^{18} W/cm^2. The polarization of the laser was in the plane of rotation of the electron spectrometer.

The electrons from the laser plasma interaction propagated through the $f/20$ lead-graphite collimator and were deflected by the electromagnet. The front side of the scintillator (BC400) is covered with two layers of thin aluminum foil. Its back side was imaged by an Andor ICCD camera. Parameters of the electron spectrometer are described in our previous paper on high density laser ponderomotive and ionization acceleration (HD-LIPA) [16]. The resolution and imaging properties of the magnet were improved by installing semicircular pole pieces. Initially, we studied the angular distribution of the injected electrons. The collimator and magnet were rotated away from the possible electron trajectories and thus the scintillator was exposed to detect electrons ejected between 0° to 50°. We checked the angular distribution for different plasma densities of helium and nitrogen gases and for different intensities of the laser. The goal was to create off-axis quasimonoenergetic electrons with moderate energy range, using as little as possible of the laser power. The most interesting angular distribution was found to be for helium plasma densities at 1.5–2 $\times 10^{19}$ cm^{-3} and laser intensity near 10^{18} W/cm^2. For this set of parameters the majority of the ejected electrons were offset from the laser propagation direction by 35°–40°, as shown in Fig. 2.

Most of the ejected electrons were concentrated in a 10° cone around the 40° line in the plane of the laser polarization. We did not check the opposite (minus 40°) direction, but we believe that the angular distribution is symmetrical in the laser polarization plane. The charge of these ejected electrons was obtained from the scintillator signal that was cross-calibrated against a fast current transformer. The total charge ejected into this 40° direction varied between 1 to 1.5 nC. All other directions in the area covered by the scintillator received less than 0.5 nC of charge.

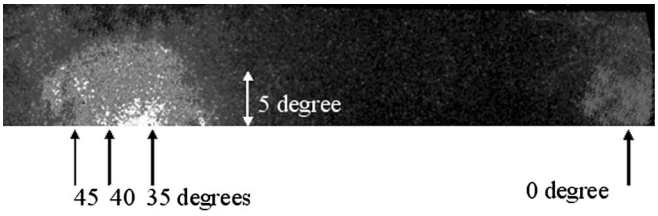

FIG. 2. Angular distribution of the ejected electrons. The scintillator is shifted up to show that the electrons are localized in the plane of the laser polarization.

The range of plasma densities and laser powers to obtain these off-axis quasimonoenergetic electrons is relatively limited. The largest angle of the ejected electrons was measured when the laser intensity was at the threshold of producing electrons, as is reported here. When the laser intensity and/or the plasma density increases two major effects were observed in the experiment: (1) electrons became diffused over a wider angle and more electrons were ejected in the laser propagation direction (zero angle), (2) the center of the cone of the ejected electrons moved toward zero angle position. Increasing of the density by a factor of 3 or increasing of the laser intensity by a factor of 2 resulted in a wide angular distribution of the electrons between 0° and 30° angle. The energy of the ejected electrons in this case was higher, but the energy spread was close to 100%, similar to previously reported measurements [16].

To obtain the energy distribution of the ejected electrons we rotated the electron spectrometer to the optimum 40° angle using the collimator. Figure 3 shows the section of the scintillator where the energy of these electrons was measured. In the absence of the magnetic field, the total charge of the electrons passing through the collimator at the 40° angle was about 500 pC. In the presence of an applied magnetic field, the high-energy segment of these electrons has a narrow energy distribution that is shown in Fig. 3. At 0.25 kG magnetic field the energy of the detected electrons was above 1.5 MeV and the total charge was above 100 pC. The measured charge was lower than the total because of the small ($\sim 3°$) acceptance angle of the collimator. However, with the collimator removed, the total charge of these energetic electrons is expected to be sub-

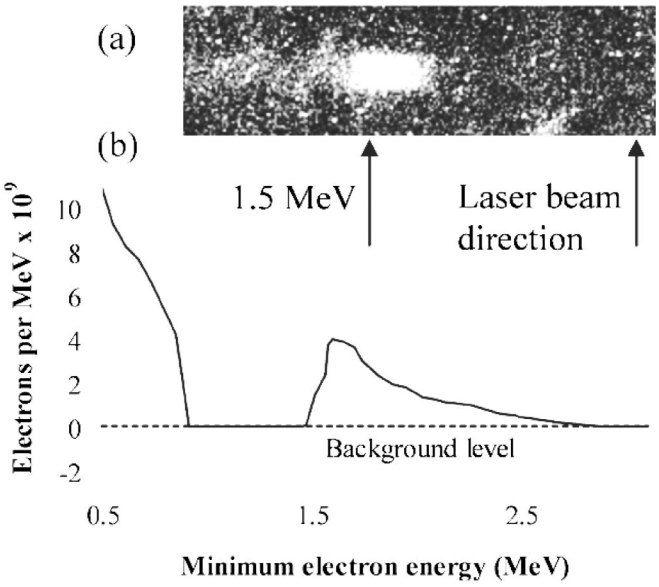

FIG. 3. Experimental electron spectrum: (a) Fragment of the scintillator images at 40° of electron spectrometer setup, magnetic field 0.25 kG, (b) electron energy distribution. The energy range and resolution are limited by the size of the scintillator.

stantially higher, since the typical acceptance angle of acceleration structure, for example, capillary, is wider than that of the collimator [12,17]. Only about 4 TW of laser power was used to create these electrons. For lower laser power the parameters of the electron beam became unstable, and for higher laser power and/or higher plasma density a wider energy distribution was measured. The 40° position on the scintillator was just a few centimeters from its edge. Therefore we had to limit the applied magnetic field to keep high-energy electrons in field of view of the scintillator. This limited the resolution of the electron spectrometer to 10% for the 2 MeV electrons.

The observed acceleration cannot be interpreted as being due to the HD-LIPA mechanism [16] because of the relatively low ionization potential of helium. Therefore, to explain the results, we carry out three dimensional fully relativistic particle-in-cell (PIC) simulations using TURBOWAVE [18] operating in the fully explicit mode (i.e., the ponderomotive guiding center approximation is not used). The plasma densities considered are 10^{19}, 2×10^{19}, and 4×10^{19} cm^{-3}. Both preionized and tunnel-ionized plasmas are considered. The plasma (or helium gas) consists of a uniform region 357 μm long, with 119 μm long transition regions on both ends. The 50 fs, 2.8 TW laser pulse is focused to a diffraction limited spot size of 5 μm ($1/e$ of the field) which corresponds to an intensity of 3×10^{18} W/cm^2. The geometric focal spot is positioned at the foot of the vacuum-plasma transition region. For the preionized runs, 4 electrons per cell are loaded into each cell with a thermal velocity of 0.01 c. For the helium runs, 4 immobile atoms are loaded into each cell, each atom potentially producing 2 electrons. In the following, z is the propagation direction and x is the polarization direction.

The main features of the simulation data are self-focusing and electron cavitation. Because of the fact that the laser pulse length is on the order of the plasma period, the critical power for self-focusing is effectively raised [19]. For this reason, in the case where the plasma density is 10^{19} cm^{-3}, self-focusing is not observed even though the nominal critical power is 1.5 TW. The wakefields generated are therefore nearly linear and no accelerated electrons are observed. However, in the case where the plasma density is 2×10^{19} cm^{-3}, the back half of the pulse is self-focused while the front half undergoes diffraction. The increased ponderomotive pressure in the back of the pulse leads to electron cavitation (bubble), as illustrated in Fig. 4. As elaborated upon below, the space charge fields associated with the cavitation region eject electrons at large angles to the propagation axis. A distinct phase space population is observed with a propagation angle of 54° and an energy of about 0.5 MeV (better agreement with the experiment was observed in one run where the intensity was increased by 20% and the pulse length was reduced to 35 fs; the propagation angle was then 38° and the energy

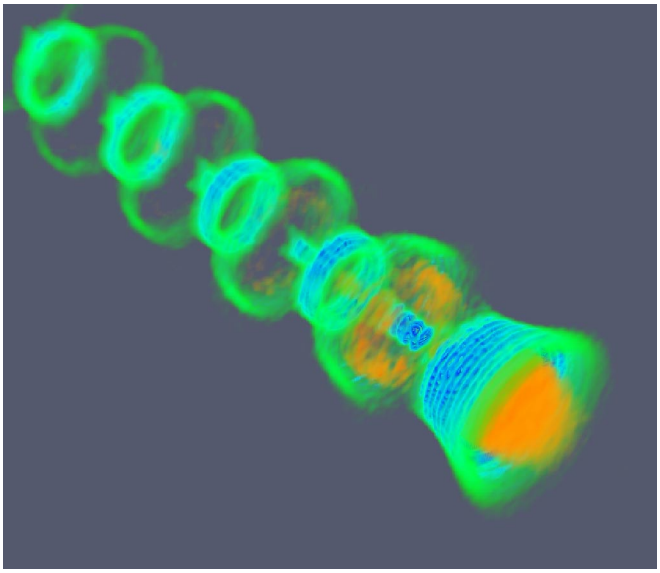

FIG. 4 (color online). Volumetric rendering of charge density behind the laser pulse as computed by turboWAVE. Orange (or light gray) is positive and blue-green (or gray) is negative. The propagation direction is down and to the right. The orange (or light gray) bubble in the lower right is the ion-rich cavitation region, and the blue-green (or gray) sheath surrounding it is a dense shell of electrons.

was 1.2 MeV). The azimuthal distribution is uniform in the preionized case, but favors the polarization direction when ionization is included. In the case where the plasma density is 4×10^{19} cm^{-3}, even stronger self-focusing occurs. However, in this case it is accompanied by the self-modulation instability. Multiple cavitation regions are observed which evolve in a complicated way. The stronger accelerating fields lead to the generation of forward directed energetic electrons. Electrons are also observed propagating at large angles, but compared to the 2×10^{19} cm^{-3} case, these are more diffused over angles and energies.

The large-angle electrons emitted in the 2×10^{19} cm^{-3} case can be interpreted as being due to the space charge fields associated with the cavitation region. This is illustrated in Fig. 5, where the orbit of a test particle is superimposed on false color images of the transverse and longitudinal wakefields. The black curve is a parametric plot of particle position with time as the parameter. The false color images correspond approximately to the field experienced by the test particle. For a test particle initially displaced toward the $-x$ axis, such as the one considered here, linear theory predicts that the ponderomotive force will first push it further in the $-x$ direction, while later in time the wakefields will push it back toward the axis. This is indeed what is seen in Fig. 5. However, the impulse due to the wake exceeds the ponderomotive impulse and the electron emerges in the $+x$ direction as an accelerated particle. This is evidently due to the strongly nonlinear

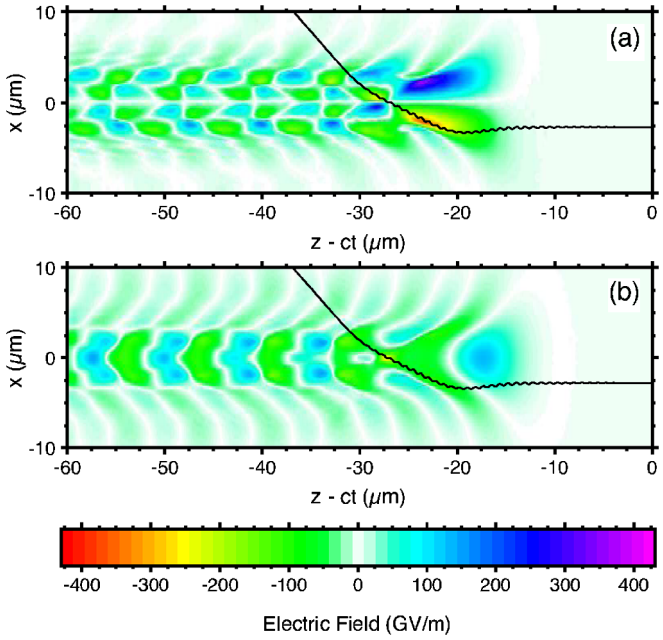

FIG. 5 (color online). Trajectory of a test electron superimposed on the wakefields produced in the 2×10^{19} cm^{-3} plasma: (a) trajectory through transverse wakefields (b) trajectory through longitundinal wakefields. The laser fields have been suppressed using a Fourier filter, though their effect is visible on the particle trajectory.

wakefields associated with the cavitation region. In particular, the transverse wakefields are strongly concentrated near the electron sheath surrounding the ion bubble. A test particle with propitious initial conditions, such as the one shown in Fig. 5, will be swept directly through the region where the field is most concentrated. In a preionized plasma, the initial conditions are isotropic and no azimuthal angle is preferred over any other. In a tunnel-ionized plasma, electrons are heated preferentially in the polarization direction. Electrons that receive a small ionization impulse become part of the sheath and are not ejected. Electrons that receive a large ionization impulse can be redirected along a trajectory just inside the sheath where the radial fields are large enough to eject them. This interpretation is confirmed by the simulations in that most of the accelerated electrons were stripped from helium ions. Because the ion has a larger ionization potential than the atom, the corresponding ionization impulse is on average larger.

In conclusion, quasimonenergetic electrons emerging from a laser wakefield accelerator at a large angle to the propagation axis have been observed experimentally and in PIC simulations. The interplay between the nonlinear structure of the cavitation wakefields, the ponderomotive force of the laser, and the tunneling ionization process, appear to be responsible for their generation. These electrons are excellent candidates for injection into the acceleration stage. The angle between the laser beam and ejected electrons makes it practical to couple the injection and acceleration stages.

This work was supported by the Department of Energy and Office of Naval Research.

*Present address: Icarus Research, Inc., Bethesda, MD, USA.
Corresponding author.
Dmitri@ppdmail.nrl.navy.mil

[1] T. Tajima and J. M. Dawson, Phys. Rev. Lett. **43**, 267 (1979).
[2] P. Sprangle, E. Esarey, A. Ting, and G. Joyce, Appl. Phys. Lett. **53**, 2146 (1988).
[3] E. Esarey, P. Sprangle, J. Krall, and A. Ting, IEEE Trans. Plasma Sci. **24**, 252 (1996).
[4] A. Pukhov and J. Meyer-ter-Vehn, Appl. Phys. B **74**, 355 (2002).
[5] A. Zhidkov, J. Koga, K. Kinoshita, and M. Uesaka, Phys. Rev. E **69**, 035401(R)(2004).
[6] F. S. Tsung *et al.*, Phys. Rev. Lett. **93**, 185002 (2004).
[7] S. P. D. Mangles *et al.*, Nature (London) **431**, 535 (2004).
[8] C. G. R. Geddes *et al.*, Nature (London) **431**, 538 (2004).
[9] J. Faure *et al.*, Nature (London) **431**, 541 (2004).
[10] J. Faure *et al.*, Nature (London) **444**, 737 (2006).
[11] W. P. Leemans *et al.*, Nature Phys. **2**, 696 (2006).
[12] D. Kaganovich *et al.*, Phys. Plasmas **12**, 100702 (2005).
[13] D. F. Gordon *et al.*, Phys. Rev. E **71**, 026404 (2005).
[14] R. F. Hubbard *et al.*, IEEE Trans. Plasma Sci. **33**, 712 (2005).
[15] C. I. Moore *et al.*, Phys. Rev. Lett. **82**, 1688 (1999).
[16] A. Ting *et al.*, Phys. Plasmas **12** 010701 (2005).
[17] D. Kaganovich *et al.*, IEEE Trans. Plasma Sci. **33**, 735 (2005).
[18] D. F. Gordon, W. B. Mori, and T. M. Antonsen, Jr., IEEE Trans. Plasma Sci. **28**, 1224 (2000); D. F. Gordon, IEEE Trans. Plasma Sci. **35**, 1486 (2007).
[19] J. Faure *et al.*, Phys. Plasmas **9**, 756 (2002).